REVIEW

Shark-skin surfaces for fluid-drag reduction in turbulent flow: a review

BY BRIAN DEAN AND BHARAT BHUSHAN*

Nanoprobe Laboratory for Bio- and Nanotechnology and Biomimetics (*NLBB*),
*Ohio State University, 201 West 19th Avenue, Columbus,
OH 43210-1142, USA*

The skin of fast-swimming sharks exhibits riblet structures aligned in the direction of flow that are known to reduce skin friction drag in the turbulent-flow regime. Structures have been fabricated for study and application that replicate and improve upon the natural shape of the shark-skin riblets, providing a maximum drag reduction of nearly 10 per cent. Mechanisms of fluid drag in turbulent flow and riblet-drag reduction theories from experiment and simulation are discussed. A review of riblet-performance studies is given, and optimal riblet geometries are defined. A survey of studies experimenting with riblet-topped shark-scale replicas is also given. A method for selecting optimal riblet dimensions based on fluid-flow characteristics is detailed, and current manufacturing techniques are outlined. Due to the presence of small amounts of mucus on the skin of a shark, it is expected that the localized application of hydrophobic materials will alter the flow field around the riblets in some way beneficial to the goals of increased drag reduction.

Keywords: shark skin; drag reduction; riblets; biomimetics; turbulent flow; hydrophobicity

1. Introduction

Nature is full of examples of structures, materials and surfaces whose traits can be exploited for commercial application. Biomimetics, meaning to mimic biology, is the study of naturally occurring properties of plants and animals for the purpose of inspired design. By studying and understanding the mechanisms of natural phenomena, we may be able to reproduce these phenomena on demand (Bhushan 2009). Efficient design is a common trait in nature, and many structures serve multiple purposes. Lotus leaves, one example of a surface with natural traits desirable in other applications, possess a hierarchical surface structure that causes superhydrophobic behaviour (Bhushan 2008, 2010; Nosonovsky & Bhushan 2008). This allows water that comes in contact with the surface to roll off easily, picking up dirt particles and cleaning the surface along the way. Rose petals are found with superhydrophobicity and either low or high adhesion (Bhushan & Her 2010). Geckos, which can walk up walls and hang upside down,

*Author for correspondence (bhushan.2@osu.edu).

One contribution of 11 to a Theme Issue 'Green tribology'.

This journal is © 2010 The Royal Society

also possess a hierarchical structure giving them controllable super-adhesion on their feet (Gorb 2001; Bhushan 2007, 2010). By creating these directional super-adhesive surfaces on legs of a robot, it is possible to create a robot that can climb walls like a gecko (Cutkosky & Kim 2009).

Nature has also created ways of reducing drag in fluid flow, evident in the efficient movement of fish, dolphins and sharks. The mucus secreted by fish causes a reduction in drag as they move through water, and also protects the fish from abrasion, by making the fish slide across objects rather than scrape, and disease, by making the surface of the fish difficult for microscopic organisms to adhere to (Shephard 1994). It has been known for many years that by adding as little as a few hundred parts per million guar, a naturally occurring polymer, friction in pipe flow can be reduced by up to two-thirds. Other synthetic polymers provide an even larger benefit (Hoyt 1975). The compliant skin of the dolphin has also been studied for drag-reducing properties. By responding to the pressure fluctuations across the surface, a compliant material on the surface of an object in a fluid flow has been shown to be beneficial. Though early studies showed dramatic drag-reduction benefits, later studies have only been able to confirm 7 per cent drag reduction (Choi *et al.* 1997).

Another set of aquatic animals that possesses multi-purpose skin is fast-swimming sharks. The skin of fast-swimming sharks protects against biofouling and reduces the drag experienced by sharks as they swim through water. The tiny scales covering the skin of fast-swimming sharks, known as dermal denticles (skin teeth), are shaped like small riblets and aligned in the direction of fluid flow (figure 1). Shark-skin-inspired riblets have been shown to provide a drag-reduction benefit up to 9.9 per cent (Bechert *et al.* 1997*b*). The spacing between these dermal denticles is such that microscopic aquatic organisms have difficulty adhering to the surface. Slower sharks are covered in dermal denticles as well, but not those that are shaped like riblets or provide any drag-reduction benefit.

The effect of riblet structures on the behaviour of fluid flow, as well as the optimization of their morphology, is the focus of this paper. To understand the mechanism of shark-skin drag reduction, it is first important to understand the nature of fluid flow over an effective shark-skin surface. Flow characteristics and the mechanism of fluid drag will be discussed for fluid flowing over a flat plate. Mechanisms of drag reduction by riblet geometries will then be discussed, followed by a review of experimental riblet studies that have been performed, a discussion of optimization data for common riblet geometries and other factors in riblet selection. Large-scale and commercial applications of riblets will then be explored, and an outlook on future research in the field will be presented.

2. Mechanisms of fluid drag

Fluid drag comes in several forms, the most basic of which are pressure drag and friction drag. Pressure or form drag is the drag associated with the energy required to move fluid out from in front of an object in the flow, and then back in place behind the object. Much of the drag associated with walking through water is pressure drag, as the water directly in front of a body must be moved out and around the body before the body can move forward. The magnitude of pressure drag can be reduced by creating streamlined shapes. Friction or viscous
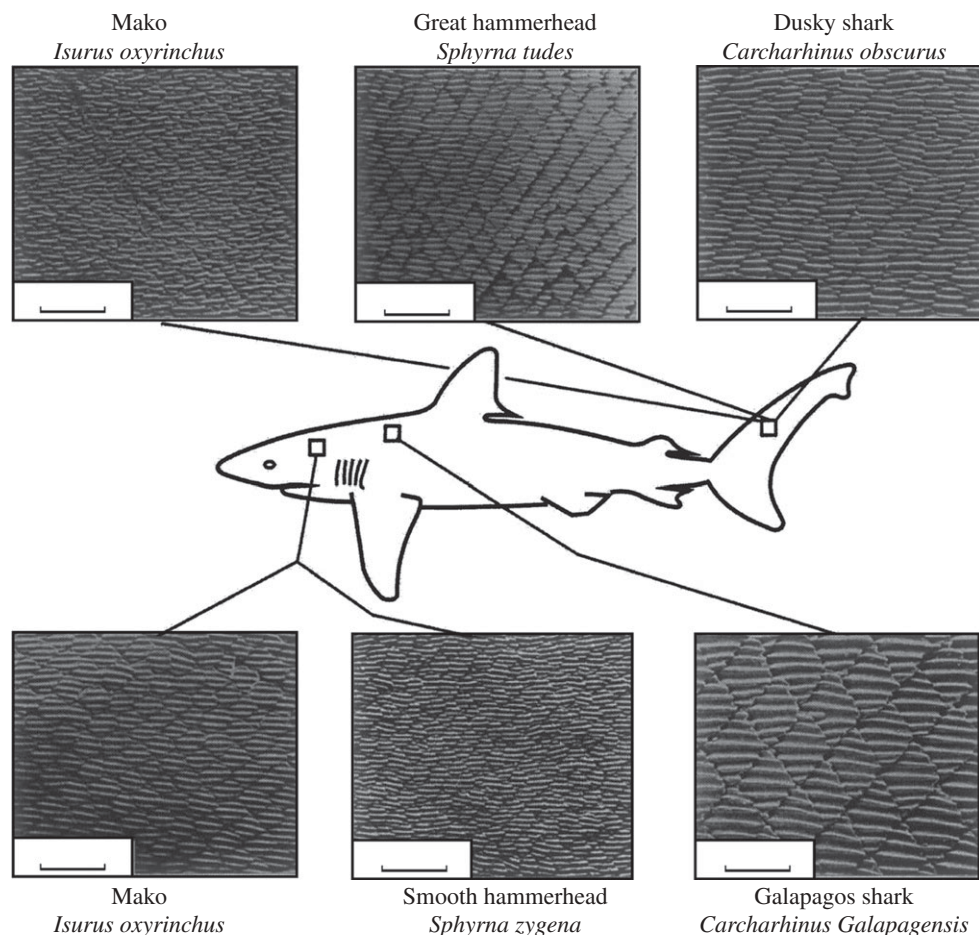
Figure 1. Scale patterns on fast-swimming sharks (adapted from Reif 1985; Bechert *et al.* 2000*a*; scale bar, 0.5 mm).

drag is caused by the interactions between the fluid and a surface parallel to the flow, as well as the attraction between molecules of the fluid. Friction drag is similar to the motion of a deck of cards sliding across a table. The frictional interactions between the table and the bottom card, as well as between each successive card, mimic the viscous interactions between molecules of fluid. Moving away from the surface of an object in a fluid flow, each fluid layer has higher velocity until a layer is reached where the fluid has velocity equal to the mean flow. Fluids of higher viscosity—the attraction between molecules—have higher apparent friction between fluid layers, which increases the thickness of the fluid layer distorted by an object in a fluid flow. For this reason, more viscous fluids have relatively higher drag than less viscous fluids. A similar increase in drag occurs as fluid velocity increases. The drag on an object is, in fact, a measure of the energy required to transfer momentum between the fluid and the object to create a velocity gradient in the fluid layer between the object and undisturbed fluid away from the object's surface.
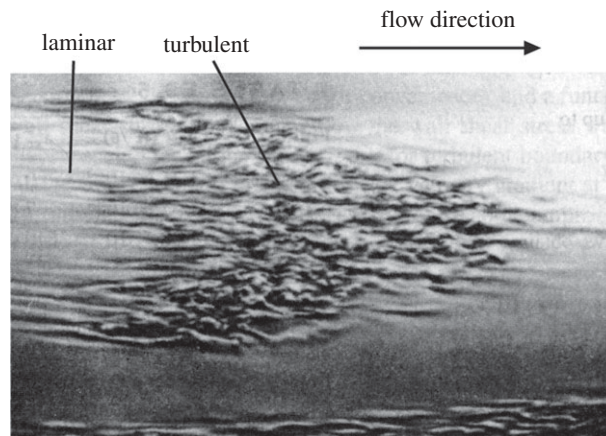
B. Dean and B. Bhushan

Figure 2. Transition between laminar and turbulent flow in fluid over a flat plate (adapted from Munson *et al.* 2005).

The above discussion of friction drag assumes all neighbouring fluid molecules move in the same relative direction and momentum transfer occurs between layers of fluid flowing at different velocities. Figure 2 shows an image of the transition between laminar flow and turbulent flow, in which molecules move in swirling and cross-stream motions such that an average velocity is maintained in the direction of flow. The inclusion of cross-flow and non-parallel relative velocities between molecules in turbulent flow causes a dramatic increase in momentum transfer. The cross-flow momentum transfer is of particular interest, as all momentum transferred parallel to the surface of an object results in a corresponding increase in drag. Natural transition occurs from laminar- to turbulent-flow regimes near a Reynolds number around 4000 for pipe flow and 500 000 for flow over a flat plate. The Reynolds number, Re, is a ratio of the inertial forces to viscous forces in a given flow. For pipe flow, $Re = \rho V D/\mu$, where ρ is the fluid density, V is the velocity, D is the pipe diameter and μ is the dynamic viscosity. For flow over a flat plate, $Re = \rho V L/\mu$, where L is the length. For values of Re much less than the transition values above, flow is laminar—dominated by viscous forces between the molecules. For larger values of Re, the flow is turbulent—dominated by inertial forces of the system (Munson *et al.* 2005).

Fully developed turbulent flow is commonly said to exhibit complete randomness in its velocity distribution, but there exist distinct regions within fully developed turbulent flow that exhibit different patterns and flow characteristics (Kline *et al.* 1967). While organization is evident in the viscous sublayer, the layer closest to the surface, the outer layers of the turbulent boundary layer are chaotic and disorganized. Much of this chaotic motion above the viscous sublayer is caused by the outward bursting of the streamwise vortices that form at the surface in the viscous sublayer. Streamwise vortices (vortices that rotate about axes in the direction of mean velocity) dominate the viscous sublayer. As these vortices rotate and flow along the surface, they naturally translate across the surface in the cross-flow direction. The interaction between the vortices and the surface, as well as between neighbouring vortices that collide during translation
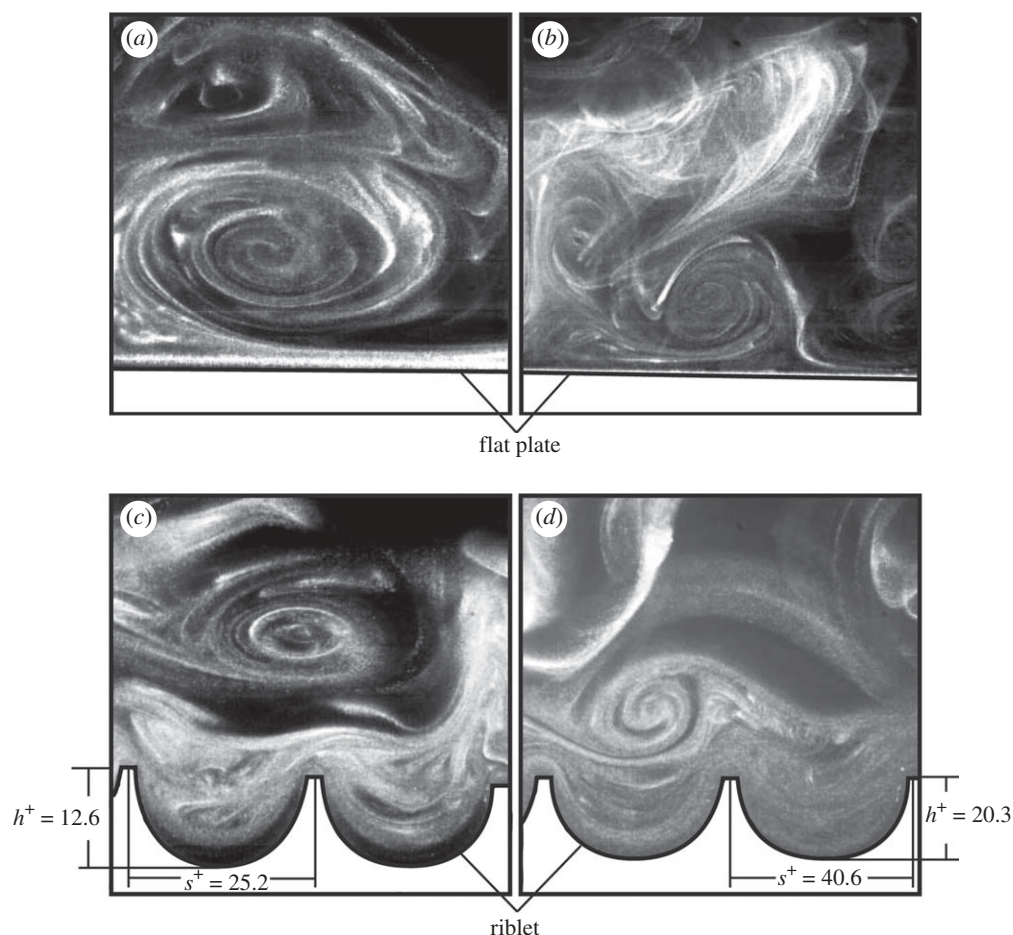
Figure 3. Turbulent-flow visualization of streamwise vortices in a vertical cross section over a flat plate: (*a*) drag decreasing case ($V = 3\,\mathrm{m\,s^{-1}}$) and (*b*) drag increasing case ($V = 5\,\mathrm{m\,s^{-1}}$). Riblet surfaces: (*c*) drag decreasing case ($V = 3\,\mathrm{m\,s^{-1}}$) and (*d*) drag increasing case ($V = 5\,\mathrm{m\,s^{-1}}$). Adapted from Lee & Lee (2001).

initiate bursting motions where vortices are rapidly ejected from the surface and into the outer boundary layers. As vortices are ejected, they tangle with other vortices and twist such that transient velocity vectors in the cross-stream direction can become as large as those in the average flow direction (Kline *et al.* 1967). The translation, bursting of vortices out of the viscous sublayer and chaotic flow in the outer layers of the turbulent boundary-layer flow are all forms of momentum transfer and are large factors in fluid drag. Reducing the bursting behaviour of the streamwise vortices is a critical goal of drag-reduction, as the drag-reduction possibilities presented by this are sizable.

The vortices were first visualized from a horizontal cross section and were seen as high- and low-speed streaks aligned in the mean-flow direction (Coles 1978). Later, a full Navier–Stokes simulation was used to replicate the high- and low-speed streaks (Robinson 1991), and more recently flow-visualization techniques were used to capture cross-sectional images, shown in figure 3, of the

streamwise vortex formations above both flat-plate and riblet surfaces (Lee & Lee 2001). The streaky structure that was seen in the horizontal cross section was representative of local average velocity flows, and is caused by interactions between neighbouring vortices. The average cross-stream wavelength of these high- and low-speed streaks, the added widths of one high-speed streak and one low-speed streak, is equal to the added diameters of two neighbouring vortices and has been measured at 70–100 wall units[1] (Kline *et al.* 1967; Wilkinson 1983; Bechert *et al.* 2000*a*). This corresponds to a vortex diameter of 35–50 wall units. Flow visualizations shown in figure 3 show vortex cross sections and relative length scales, demonstrating vortex diameters smaller than 40 wall units (Lee & Lee 2001).

3. Role of riblets in drag reduction

The small riblets that cover the skin of fast-swimming sharks work by impeding the cross-stream translation of the streamwise vortices in the viscous sublayer. The mechanism by which the riblets interact with and impede vortex translation is complex, and the entirety of the phenomena is not yet fully understood. On a practical level, impeding the translation of vortices reduces the occurrence of vortex ejection into the outer boundary layers as well as the momentum transfer caused by tangling and twisting of vortices in the outer boundary layers.

One classical cause of increased drag that shark-skin-mimicking riblet surfaces exhibit is an increase in wetted surface area. In the turbulent-flow regime, fluid drag typically increases dramatically with an increase in surface area owing to the shear stresses at the surface acting across the new, larger surface area. However, as vortices form above a riblet surface, they remain above the riblets, interacting with the tips only and rarely causing any high-velocity flow in the valleys of the riblets. Since the higher velocity vortices interact only with a small surface area at the riblet tips, only this localized area experiences high-shear stresses. The low-velocity fluid flow in the valleys of the riblets produces very low-shear stresses across the majority of the surface of the riblet. By keeping the vortices above the riblet tips, the cross-stream velocity fluctuations inside the riblet valleys are much lower than the cross-stream velocity fluctuations above a flat plate (Lee & Lee 2001). This difference in cross-stream velocity fluctuations is evidence of a reduction in shear stress and momentum transfer near the surface, which minimizes the effect of the increased surface area. Though the vortices remain above the riblet tips, some secondary vortex formations do occur that enter the

[1]As flow properties change, the dimensions of the turbulent-flow structures change as well. As such, it is useful to use non-dimensional length values to better compare studies performed in different flow conditions. Dimensionless wall units, marked $^+$, are used for all length scales, which are calculated by multiplying the dimensional length by V_τ/ν. For example, $s^+ = s V_\tau/\nu$, where s^+ is the non-dimesional riblet spacing, s is the dimensional riblet spacing, ν is the kinematic viscosity and $V_\tau = (\tau_0/\rho)^{0.5}$ is the wall stress velocity, for which ρ is the fluid density and τ_0 is the wall shear stress. Wall shear stress can be estimated for round-pipe flow using the equation $\tau_0 = 0.03955\nu^{1/4}\rho V^{7/4}d^{-1/4}$, where V is the average flow velocity and d is the hydraulic diameter. For flow in rectangular pipes, the equation for hydraulic diameter $d = 4A/c$ can be applied, where A is the cross-sectional area and c is the wetted perimeter.
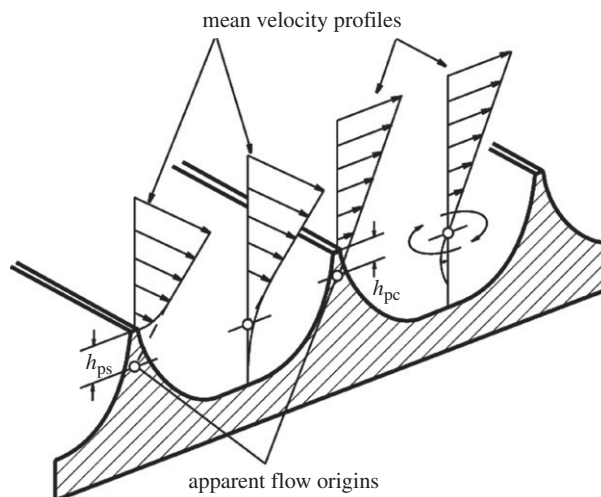
Figure 4. Schematic of the mean velocity profiles and effective protrusion heights for flow in both the streamwise direction, h_{ps}, and in the cross-flow direction, h_{pc} (adapted from Bechert *et al.* 1997*b*).

riblet valleys transiently. The flow velocities of these transient secondary vortices are such that the increase in shear stress caused by their interaction with the surface of the riblet valleys is small.

Protruding into the flow without greatly increasing fluid drag allows the riblets to interact with the vortices to reduce the cross-stream translation and related effects. As the riblets protrude into the flow field, they raise the effective flow origin by some distance. The amount by which the height of the riblets is greater than the apparent vertical shift of the flow origin is referred to as the effective protrusion height. By calculating the average streamwise velocity in laminar flow at heights over riblet surfaces and comparing them to the average streamwise velocities in laminar flow at heights over a flat plate, the effective streamwise protrusion height, h_{ps}, is found for laminar flow. The effective cross-stream protrusion height, h_{pc}, is similarly found for laminar flow by comparing the cross-stream velocities over a riblet surface with those over a flat plate. A schematic of streamwise and cross-stream flow-velocity profiles and effective protrusion heights is shown in figure 4. The difference between the vertical shifts in the streamwise and cross-stream origin, $\Delta h = h_{ps} - h_{pc}$, for any riblet geometry has been proposed to be the degree to which that riblet geometry will reduce vortex translation for low *Re* flows (Bechert *et al.* 1997*b*). As the *Re* increases, the degree to which increased surface area affects the overall fluid drag increases, and the drag-reduction correlation to these laminar-flow theories deteriorates.

Numerical modelling of turbulent flow over riblet systems has also been done (Goldstein *et al.* 1995). Using an immersed-boundary technique, a virtual riblet surface was created in turbulent flow inside a duct. This technique involves the insertion of point forces in the flow arranged in the shape of the desired riblet surface, which exert a stalling force opposite the direction of flow. Due to the random nature of fluid velocities in turbulent flow, a feedback loop must be used to adjust each point force to create an equilibrium state of zero velocity fluid in the shape of the riblet surface. Using this modelling method, the response of inserting
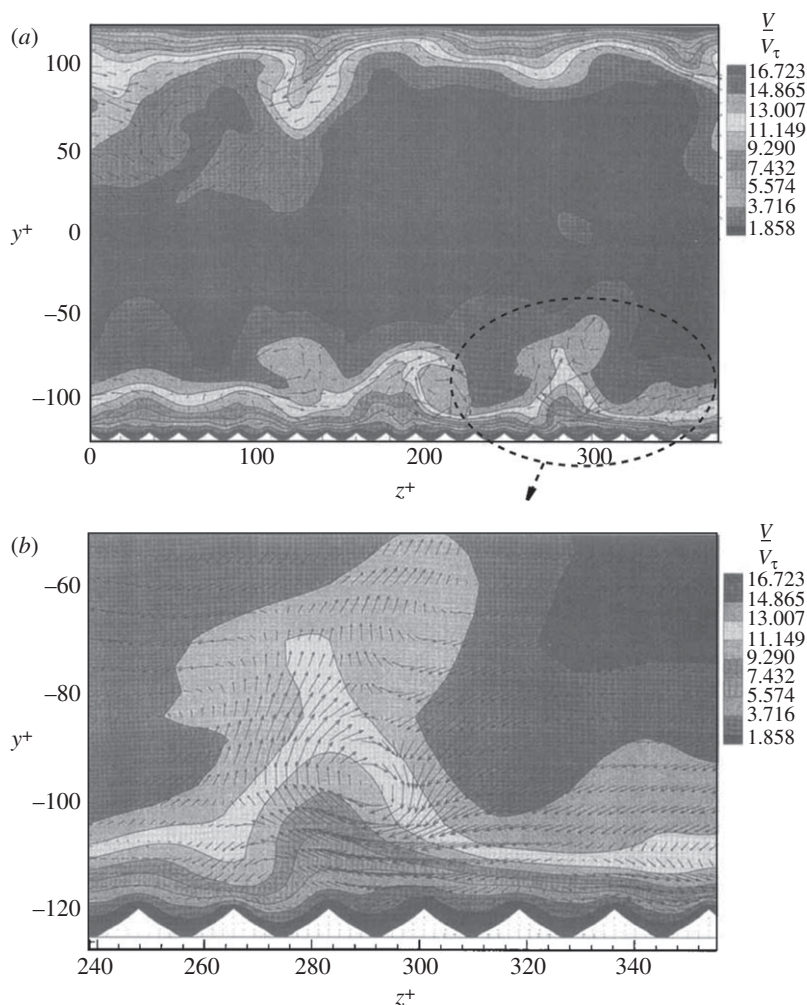
Figure 5. Plots showing numerically simulated flow through a duct with a virtual riblet surface on the bottom and a flat surface on the top. A magnified view of a region of interest from the duct in (a) is shown in (b). Virtual riblets have a sawtooth cross section with $h/s \sim 0.29$. Non-dimensionalized length scales used for dimensions parallel and normal to the surfaces are z^+ and y^+, respectively. Lines of constant velocity are shown, as well as velocity vectors. Regions of similar flow velocity are plotted using a ratio of velocity, V, to wall stress velocity $V_\tau = (\tau_0/\rho)^{0.5}$ (adapted from Goldstein et al. 1995).

a riblet surface into a turbulent flow can be monitored to better understand the mechanisms of drag reduction. In their study, Goldstein et al. (1995) first inserted virtual flat-plate boundaries in laminar and turbulent flow over a flat plate. These tests benchmarked the capability of the point forces to accurately represent a stagnant boundary in steady flow and the capability of the feedback loop to accurately model a boundary in unsteady flow, respectively. Building from these platforms, two virtual riblet surfaces were tested in turbulent flow. Velocity contours from one of these virtual riblet surfaces can be seen in figure 5. These surfaces performed similarly to similar physical riblet surfaces, and showed up to

3.3 per cent drag reduction when compared with a flat surface. Analysis of the modelled flow fields over the riblet surfaces is in consensus with existing theories of drag-reduction mechanisms. As vortices form on the surface, they remain above the riblet tips, which creates a low-velocity channel in the riblet valleys. The low-velocity channel between riblet tips has a lower velocity gradient than flow over a flat plate, which reduces shear stresses over most of the riblet surface. Velocity gradients are higher at the riblet tips, and shear stresses are correspondingly higher. The net result of this shear-stress distribution is a favourable decrease in overall drag. Also, vortex translation across the riblet surface during animations was noticeably damped in comparison to flow over a flat plate. Damped vortex translation serves to reduce the occurrence of vortex bursting, tangling and outer-layer turbulence.

4. Optimization of riblet geometry

The cross-sectional shape of riblets on fast-swimming sharks varies greatly, even at different locations on the same shark. Figure 1 shows the difference between the separated blade riblets on the tail of a Shortfin Mako shark, *Isurus oxyrinchus*, with the scale-grouped riblets on its front section, as well as the morphology that exists on various other fast-swimming sharks. Many types of riblets have been studied, the shapes of which have been chosen for several reasons. Riblet shapes have been chosen for their similarity to natural riblets, for their ease of fabrication and for purposes of drag-reduction optimization. Two-dimensional riblets, which have a continuous extrusion of a simple cross section in the streamwise direction, have been most extensively characterized. The most thorough characterization has been completed for symmetrical two-dimensional riblets with sawtooth, scalloped and blade cross sections, as shown in figure 6 (Walsh 1980, 1982; Walsh & Lindemann 1984; Bechert & Hoppe 1985; Bechert *et al.* 1986, 1997*a*, 2000*a,b*; Wilkinson & Lazos 1987; Wilkinson *et al.* 1988; Walsh & Anders 1989). Alternative riblet geometries have, in general, shown no increased benefit. These riblets, including asymmetrical riblets, hierarchical riblets and riblets with rounded or notched peaks have been studied in detail and do not improve upon the benefit of standard driblet geometries (Walsh 1980, 1982; Walsh & Lindemann 1984). Other two-dimensional riblet shapes that have been studied include alternating brother–sister type riblets (Bechert *et al.* 1997*a*) and hierarchical riblets with small riblets on top of larger riblets (Wilkinson & Lazos 1987). Three-dimensional riblets, which include segmented two-dimensional riblets as well as shark-skin mouldings and replicas have also been studied. Riblet types characterized include aligned segmented-blade riblets (Wilkinson & Lazos 1987), offset segmented-blade riblets (Bechert *et al.* 2000*a*), offset-three-dimensional blade riblets (Bechert *et al.* 2000*a*) and three-dimensional shark-skin replicas (Bechert *et al.* 2000*b*; Lang *et al.* 2008; Jung & Bhushan 2010).

Most studies are done by changing the non-dimensionalized spacing, s^+, by varying only fluid velocity and collecting shear-stress data from a shear-stress balance in a wind tunnel or fluid-flow channel. Pipe-flow tests will be discussed as well. Measured shear stress is compared with shear stress over a flat plate and plotted against the calculated s^+ value for the flow conditions. In this manner, a performance curve is created for a riblet array with a
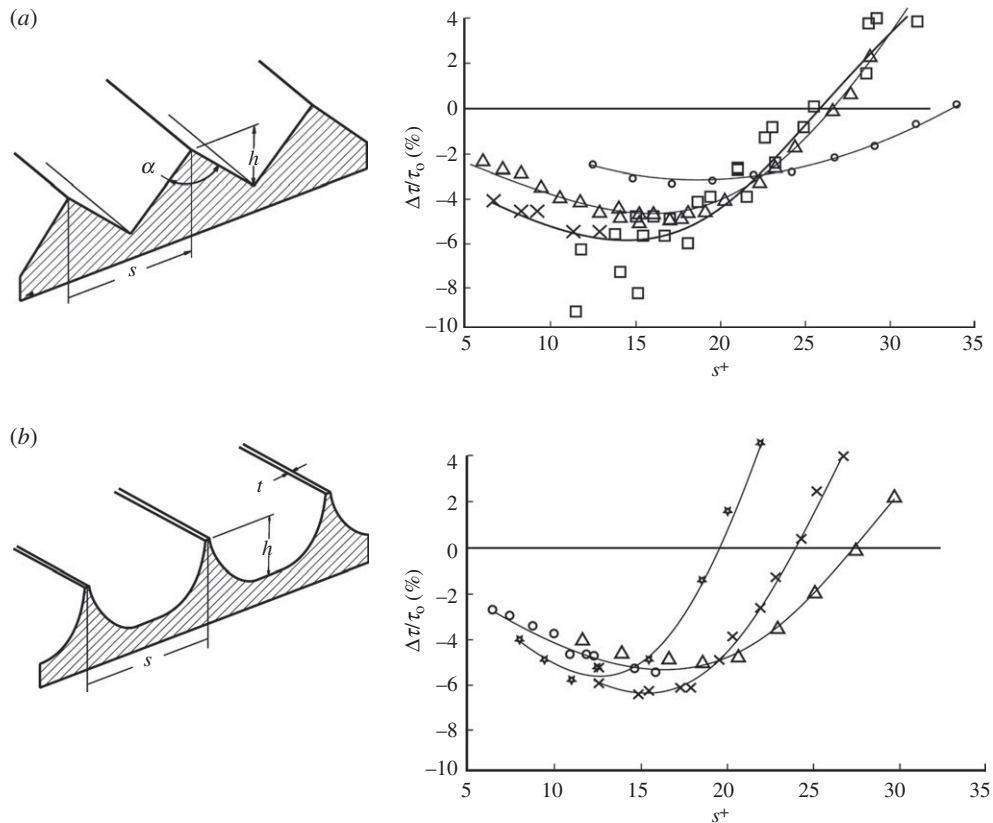
Figure 6. (a) Schematic of riblet dimensions and drag-reduction dependence on α for sawtooth riblets. The optimum drag reduction for sawtooth riblets is around $\alpha = 54°$. For $\alpha = 54°$, the best-fit line spans two datasets which overlap (cross symbols: $\alpha = 54$, $h/s = 0.98$ (adapted from Bechert et al. 1997b); open squares: $\alpha = 54$, $h/s = 0.98$ (adapted from Walsh 1982); open triangles: $\alpha = 60$, $h/s = 0.98$ (adapted from Bechert et al. 1997b); open circles: $\alpha = 90$, $h/s = 0.98$ (adapted from Bechert et al. 1997b)). (b) Schematic of riblet dimensions and drag-reduction dependence on h/s ratio for scalloped riblets. The optimum drag reduction for scalloped riblets is around $h/s = 0.7$. For $h/s = 0.5$, the best-fit line spans two datasets which overlap (open circles and triangles, $h/s = 0.5$; cross symbols, $h/s = 0.7$; stars, $h/s = 1.0$; all adapted from Bechert et al. 1997b). (c) Schematic of riblet dimensions and drag-reduction dependence on h/s ratio and thickness for blade riblets. Optimum drag reduction for blade riblets occurs at $h/s = 0.5$. Riblet-thickness experiments carried out at $h/s = 0.5$ show thinner riblets provide an improved drag-reduction benefit. Blade thickness was changed by inserting thinner blades in place of original blades. (i) blade riblets h/s optimization $t/s = 0.04$ and (ii) blade riblet thickness optimization $h/s = 0.5$ (both adapted from Bechert et al. 1997b).

specific set of characteristic dimensions. The use of non-dimensional characteristic dimensions for riblet studies, namely non-dimensional spacing, s^+, is important for comparison between studies performed under different flow conditions. Non-dimensionalization accounts for the change in size of flow structures like vortex diameter, which is the critical value to which riblets must be matched. Experiments have been carried out with various surface materials and in air,

(*c*)

blade riblet *h/s* optimization

(i)

max: −9.01% (*h/s* = 0.6)

(ii) blade riblet thickness optimization

s^+
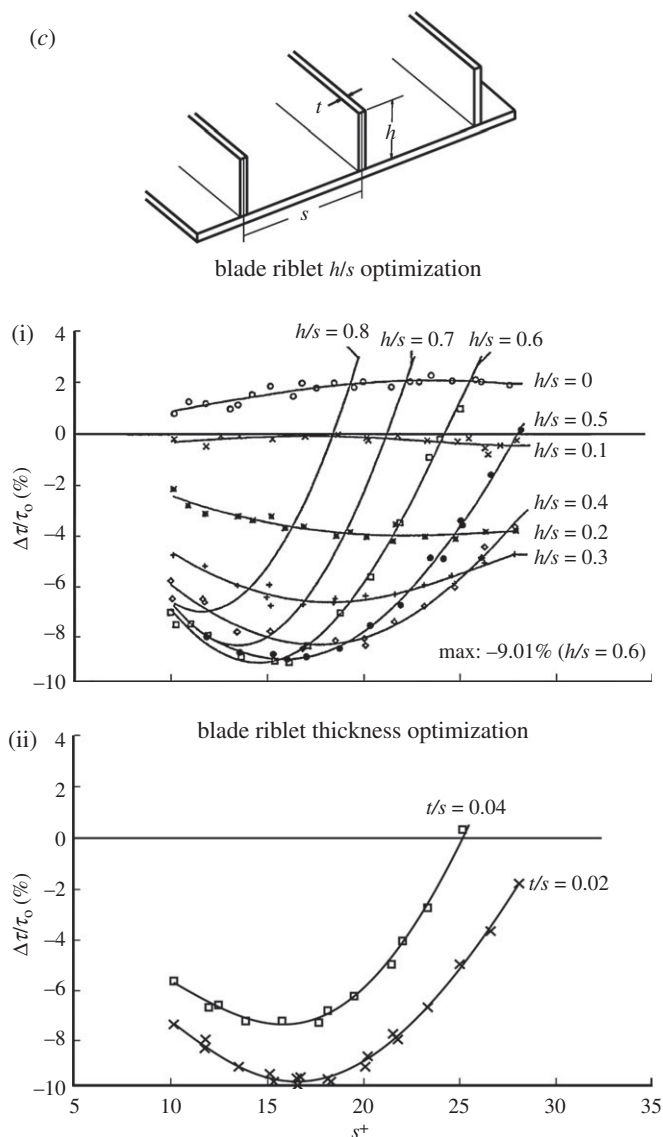
Figure 6. (*Continued*).

oil and water. Under the same non-dimensionalized flow conditions, riblet arrays sharing characteristic dimension ratios create similar performance curves whether they are made of different materials, are tested in different fluids or fabricated at a different scale.

(*a*) Optimization of two-dimensional riblets

Sawtooth riblets are the most commonly studied riblets. A schematic with characteristic dimensions and optimization data is shown in figure 6*a*. Sawtooth riblets are defined either by their height-to-spacing (h/s) ratio or their peak
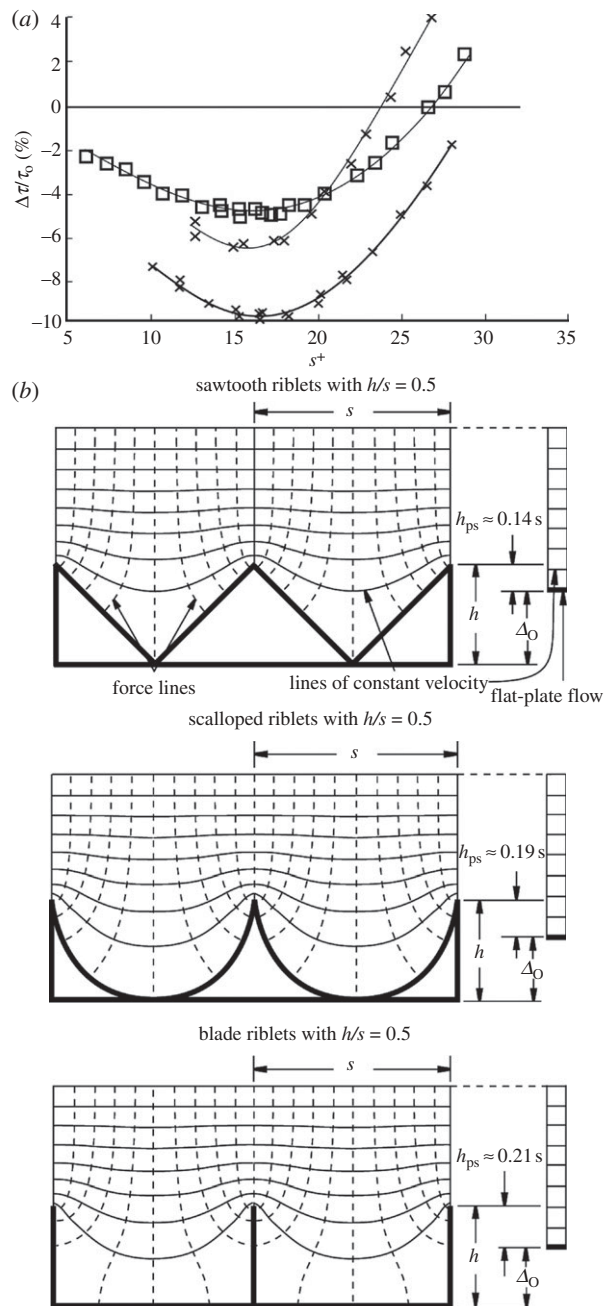
Figure 7. (*Caption opposite.*)

angle, α. The best-fit line for riblets with $\alpha \sim 54°$ was drawn spanning overlapping datasets from different sources. From available data, the optimal sawtooth riblets provide about 5 per cent drag reduction at $h/s \sim 1.0$ and $\alpha = 54°$ (Bechert *et al.* 1997*b*).

Figure 7. (*Opposite.*) (*a*) Drag-reduction comparison for sawtooth, scalloped and blade riblets with $h/s = 0.5$ (open square: sawtooth, $h/s = 0.86$, $\alpha = 60$; cross symbols: scalloped, $h/s = 0.7$; filled circle: blade, $h/s = 0.5$, $t/s = 0.02$; data from Bechert *et al.* (1997*b*)). (*b*) Schematic of lines of constant velocity above riblet and flat-plate surfaces in laminar flow allow for a comparison of effective protrusion height, h_{p}, of sawtooth, scalloped and blade riblets. The effective protrusion height, which is favourable for the reduction of vortex-translation reduction, is the difference between the riblet height, h, and the upward shift in the effective flow origin, Δ_{O}; $h_{\mathrm{p}} = \Delta_{\mathrm{O}} - h$. To find the upward shift in the effective flow origin, the height and velocity of the lowest undisturbed line of constant velocity above a riblet surface are determined. Next, the height at which flow over a flat plate reaches the same velocity is determined. The difference between these two heights is the upward shift in the effective flow origin. Blade riblets have the largest effective protrusion height. Scalloped riblets have the second largest, and sawtooth riblets have the lowest of the three (adapted from Bechert *et al.* 1986, 1997*b*).

Scalloped riblets are most commonly defined by their h/s ratio, but test shapes have varied between research groups. While the basic shapes are similar, no consensus has been formed about a standard scalloped profile. Generally, any concave shape may be referred to as scalloped and comparing data between sawtooth-, scalloped- and blade-riblet optimizations will support a generalization of comparable shapes. Ideally, the tip of the riblet is thin and sharp, but scalloped riblets with measurable tip thicknesses have also produced favourable results. Figure 6*b* shows optimization data for scalloped riblets. A maximum drag reduction of 6.5 per cent has been achieved for scalloped riblets with $h/s \sim 0.7$ (Bechert *et al.* 1997*b*).

Blade riblets have been rigorously studied in their characteristic dimension ratios. A schematic with characteristic dimensions and optimization data for blade riblets is in figure 6*c*. By fabricating an adjustable blade-riblet test stand, a 9.9 per cent drag reduction was achieved with optimized dimensions of $h/s \sim 0.5$ and $t/s = 0.02$ was found (Bechert *et al.* 1997*b*). Due to their inherent weak structure, optimal blade riblet thickness is limited by strength, not fluid dynamics. Blades that are too thin will warp in fluid flow and allow vortices to translate as a result.

When comparing the optimal drag-reduction geometries for sawtooth, scalloped and blade riblets shown in figure 7*a*, it is clear that blade riblets provide the highest level of drag reduction, scalloped riblets provide the second most, and sawtooth riblets provide the least benefit. A summary of comparison features for sawtooth, scalloped and blade riblets is given in table 1. In general, it can be seen in figure 6 that each type of riblet is most beneficial near $s^+ \sim 15$, which is between one-third and one-half of the width of the streamwise vortices. Larger s^+ will cause vortices to begin falling into the gap between the riblets, which increases the shear stress at the surface between riblets. As s^+ decreases below optimum, the overall size of the riblets decreases to a point below which they cannot adequately impede vortex translation.

Comparing drag-reduction benefit potential to effective protrusion height in the streamwise direction, it is apparent that increased protrusion height is correlated to drag-reduction potential. Figure 7*b* shows the effective streamwise protrusion height for sawtooth, scalloped and blade riblets. For the same h/s, blade riblets have the smallest shift in the effective flow origin owing to their small cross-sectional area, and sawtooth riblets have the largest shift in the effective
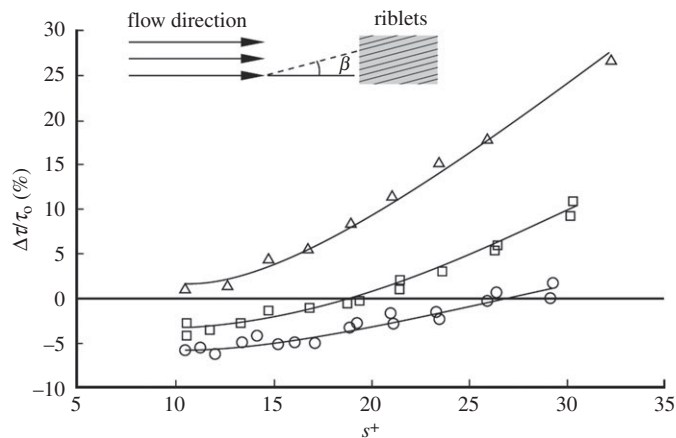
Figure 8. Drag-reduction dependence on yaw angle, β, of sawtooth riblets in free stream for $h/s \approx 0.62$ (adapted from Walsh & Lindemann 1984). Open circles, $\beta = 0$; open squares; $\beta = 15$, open triangles, $\beta = 30$.

Table 1. Summary and comparison of optimum riblet geometry for various riblet shapes.

riblet shape	relative rank[a]	maximum drag reduction (%)[b]	optimum geometry[b]	comments
sawtooth	3	5	$h/s \sim 1$, $\alpha \sim 60°$	most durable
scalloped	2	6.5	$h/s \sim 0.7$	
blade	1	9.9	$h/s \sim 0.5$	drag reduction increases as riblet thickness decreases; durability is an issue

[a]1 corresponds to greatest drag reduction.
[b]Based on the published data in Bechert *et al.* (1997*b*).

flow origin. Though all three profiles share a calculated maximum streamwise protrusion height of 0.2206 s at separate values of h/s, an increase in overall drag is experienced at these values owing to the increased drag contributions of surface shear-stress effects on the increased surface area in the turbulent regime (Bechert *et al.* 1986). The height at which h_p is maximized causes such an increase in effective flow origin shift that the drag-reduction benefits are outweighed.

An additional concern to the application of riblets is the sensitivity of drag reduction to yaw angle. Yaw angle, the angle between the average flow direction and the riblet orientation, has a deleterious effect on the drag-reduction benefits of riblet surfaces. Riblet surfaces become drag inducing above $\beta = 30°$, but small drag reductions can still be seen up to $\beta = 15°$ (Walsh & Lindemann 1984). Figure 8 shows the effects of yaw angle on riblet performance for flow over sawtooth riblets.

(b) Studies with three-dimensional riblets

Riblets on shark skin exist in short segments and groups, not as continuous structures. Riblets with three-dimensional features have been created to better approximate the performance of actual shark skin and to determine whether
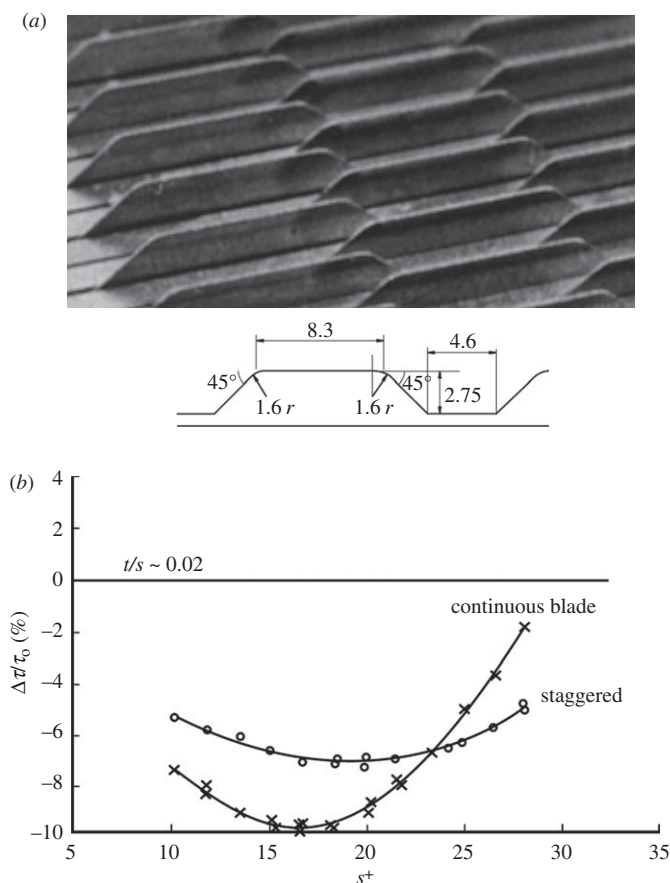
Figure 9. Comparison of drag reduction over optimum continuous blade riblets with optimum segmented trapezoidal blade riblets. (*a*) Segmented riblets were staggered as shown. Spacing between offset rows is $s/2$, while spacing between corresponding rows is s. (*b*) Optimal h/s ratio is shown for staggered blade riblets (cross symbols, $h/s = 0.5$). Optimal h/s ratio is shown for continuous blade riblets (open circles, $h/s = 0.4$). Staggered blade riblets provide less drag-reduction benefits than continuous blade riblets (adapted from Bechert *et al.* 1997*b*, 2000*a*).

there are methods of drag reduction not yet understood from two-dimensional riblet studies. Studies have explored the effects of compound riblet structures and three-dimensional riblets comprised of aligned, segmented-blade riblets (Wilkinson *et al.* 1988). No improvement in net drag reduction was realized when compared with the corresponding performance of continuous riblet geometries. More recently, experiments with similarly shaped segmented-blade riblets at spacing s with a matching set of segmented-blade riblets staggered between each row of blades at a spacing of $s/2$ from either side have been performed (Bechert *et al.* 1997*b*). A schematic and image of staggered trapezoidal blade riblets is shown in figure 9*a*. Using these and other staggered riblets, Bechert *et al.* (1997*b*) hoped to achieve the same vortex elevation and anti-translation effects of continuous riblets with less effect on the flow origin. Experimental data comparing the largest drag reduction achieved with staggered segmented-blade

riblets to optimum continuous blade riblets can be seen in figure 9*b*. Again, no net benefit in drag reduction was achieved, and after comparison of data, the conclusion was made that it is unlikely that three-dimensional riblets comprised of segmented two-dimensional riblets will greatly outperform continuous two-dimensional riblets.

In the true three-dimensional realm, it has been theorized for some time that scales on which shark-skin riblets are commonly grouped contribute to the performance of some shark-skin varieties. By creating a pressure-exchange system below the scale surface, it was theorized that injection methods may have a pressure-streak cancellation effect in the viscous sublayer, but concluded that the increased momentum exchange created would have deleterious effects (Wilkinson 1983; Bechert & Hoppe 1985; Bechert *et al.* 1986). More recently, there have been studies that have investigated the drag-reduction properties of riblet-topped shark scales as both a static structure (Jung & Bhushan 2010) and a flexible— possibly controllable—member (Lang *et al.* 2008). Using the scales moulded in epoxy resin from the skin of the Spiny dogfish (*Squalus acanthias*), shown in figure 10*a*, Jung & Bhushan (2010) have achieved a decrease in pressure drop—corresponding to a decrease in fluid drag—versus a smooth surface in a rectangular flow-cell flow experiment. Pressure drop from inlet to outlet of a pipe is a measure of drag, with a large pressure drop occurring as a result of high drag. In addition to the first study, a minimal decrease in pressure drop was realized in a similar experiment using segmented aligned riblets fabricated on acrylic (figure 10*b*) compared with a smooth acrylic test section. Results of the moulded epoxy scale study are shown in figure 11*a*, and results from the segmented-blade riblet study are shown in figure 11*b*. Certain sharks are known to exhibit riblet-topped scales that are attached somewhat flexibly to the underlying surface of the shark skin. These scales are able to change their pitch angle by bristling. As the pressure beneath the scale attachments changes, the flexible member changes position, and the trailing edge of the scales can lift up. Alternatively, the scales may bristle at concave skin locations that occur during the natural swimming. In an experiment simulating the bristling of flexible riblet covered scales into the boundary layer as a possible mechanism of control and drag reduction, no drag-reduction benefit was achieved through extreme scale bristling. However, notable flow phenomena were found to occur as a result of scale bristling, including the formation of three distinct vortex shapes (Lang *et al.* 2008).

(*c*) Riblet trends in pipe flow

Riblet effects in pipe flow have been studied as well, and general patterns exist in the drag-reduction benefit of sawtooth riblets. Due to the difficulty of riblet application in pipes, data are generally limited to applications of sawtooth-riblet film produced by 3M (Liu *et al.* 1990; Rohr *et al.* 1992). Drag-reduction tests in pipe flow are carried out by comparing the pressure drop in a riblet-lined pipe with that of a similar pipe with a smooth surface. Drag-reduction data for sawtooth riblets on a flat plate are shown in figure 12*a*, and drag-reduction data for water flow in sawtooth-riblet-lined pipes are shown in figure 12*b*. As riblets are applied to the inside surface of a pipe, the riblet tips are shifted together owing to the curve of the pipe wall. Consequently, the optimized s^+ range for riblets in pipe

(*a*) shark-skin (*Squalus acanthias*) replica

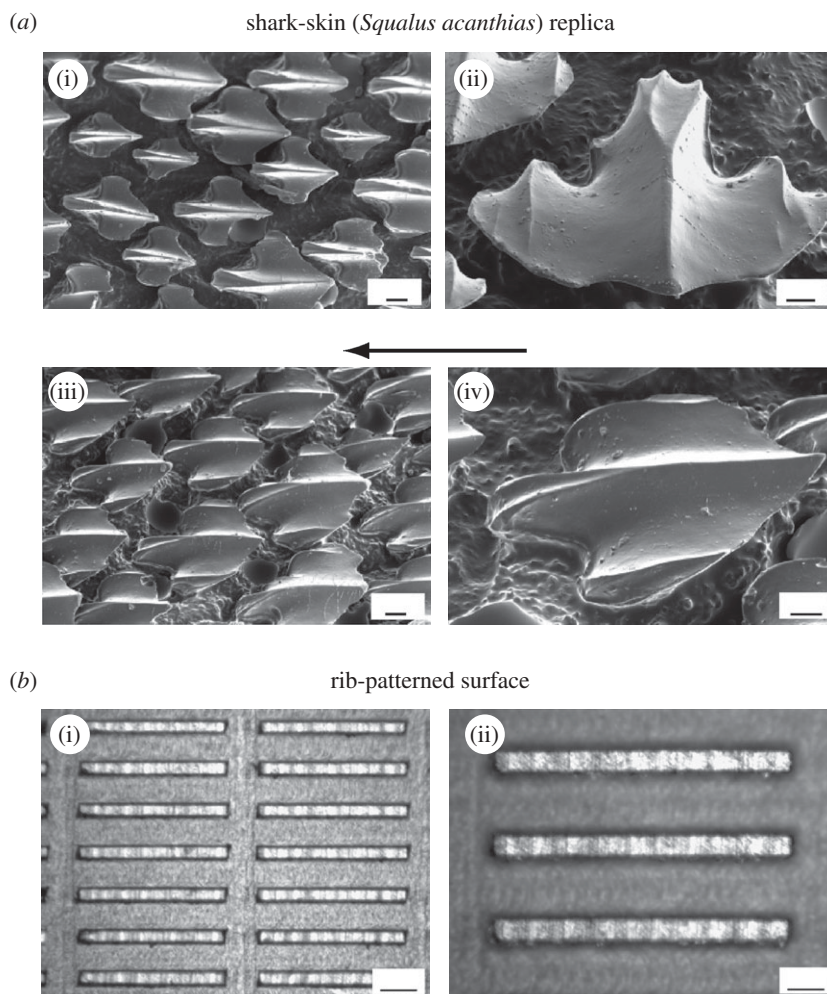(*b*) rib-patterned surface

Figure 10. (*a*) Scanning electron microscope (SEM) micrographs of shark-skin replica patterned in epoxy ((i) top view; (ii) 45° tilt-angle side view; (iii,iv) 45° tilt-angle top view (swimming direction); scale bars, (i,iii) 100 μm; (ii,iv) 50 μm). (*b*) Segmented-blade-style riblets fabricated from acrylic (scale bars, (i) 200 μm; (ii) 100 μm; adapted from Jung & Bhushan 2010).

flow is lower than that for the same riblets in flow over a flat surface (Liu *et al.* 1990). Additionally, the decrease in s^+ suggests that an increased drag reduction in round pipes might be seen with a larger characteristic angle, α, than for flow over riblets on a flat surface.

5. Riblet fabrication and applications

Riblet manufacture for study and large-scale applications has been one of the main difficulties in the field. Typical microscale manufacturing techniques are ill-fitted for large-scale application owing to the associated costs. Even for study,
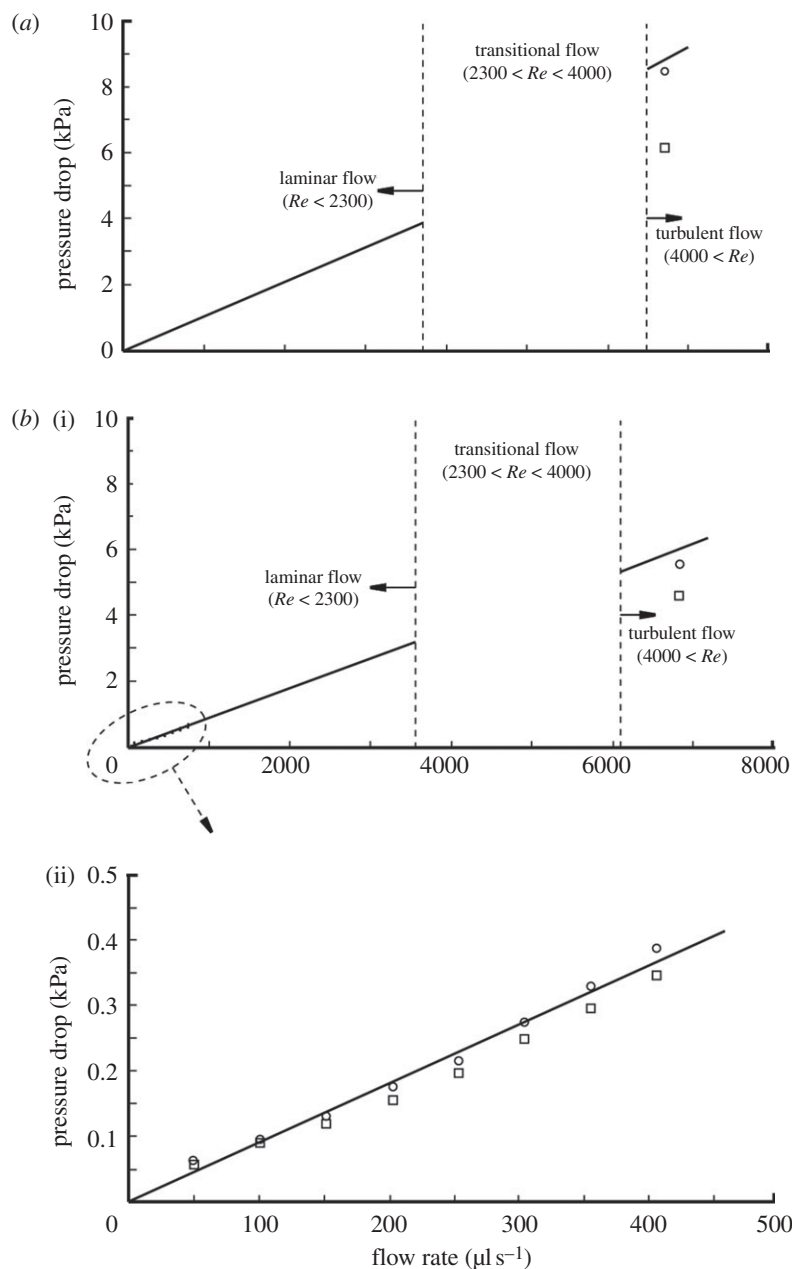
Figure 11. (*a*) Comparison of pressure drop in rectangular pipe flow over a flat epoxy surface with a shark-skin replica surface (solid line, predicted for hydrophilic surface; open circle, flat epoxy resin; open square, epoxy shark-skin replica). (*b*) Comparison of pressure drop in rectangular pipe flow over a flat acrylic surface and segmented-blade riblets (solid line, predicted for hydrophilic surface; open circle, flat acrylic surface; open square, three-dimensional riblet patterned surface). Data are compared with the predicted pressure-drop function for a hydrophilic surface (adapted from Jung & Bhushan 2010).
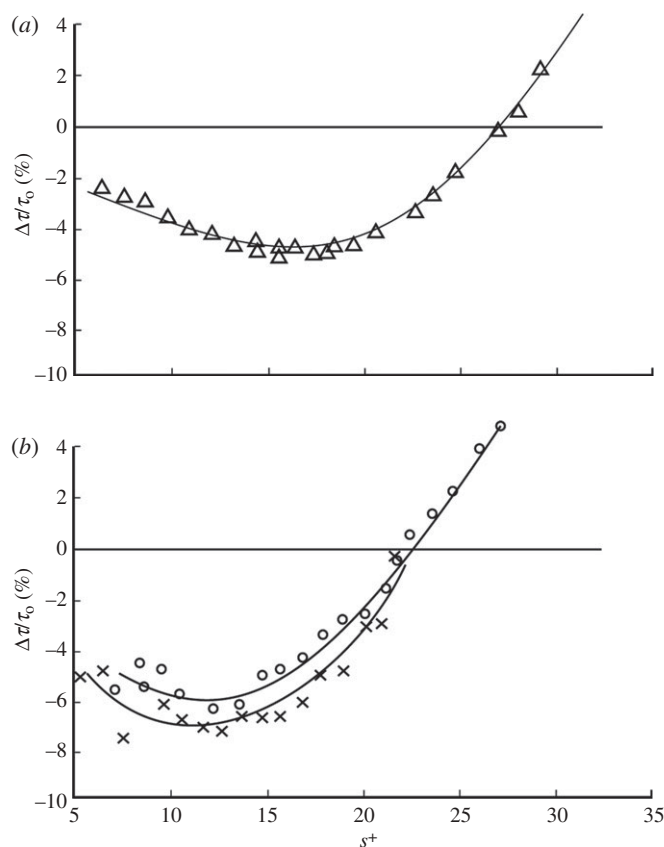
Figure 12. Comparison of riblet performance curves over sawtooth riblets on a flat-plate surface (*a*) and inside round pipes (*b*) of 25.4 mm and 50.8 mm diameters. Peak drag reduction for riblets in pipe flow occurs near $s^+ = 12$, which is lower than the flat-plate optimal value of $s^+ = 15$ (open triangle: $\alpha = 60$, $h/s = 0.86$; open circle: $\alpha = 60$, $h/s = 0.86$, pipe $D = 25.4$ mm; cross symbols: $\alpha = 60$, $h/s = 0.86$, pipe $D = 50.8$ mm; adapted from Liu *et al.* (1990) and Bechert *et al.* (1997*b*)).

most researchers have opted for traditional milling or moulding methods over the microfabrication techniques used in the microtechnology industry. Though non-dimensional units allow for comparison between flow fields of different fluids and at different conditions, the accurate microscale manufacture of riblets for experimentation has been a field of study in its own right. The largest difficulty in optimizing riblet geometries has been the fabrication of riblet series with incremental changes in characteristic dimension. Riblets used in air flow require spacings at or below 1 mm owing to the low viscosity of air and the high speed at which wind tunnels must operate to create accurately measurable shear stresses on a test surface. Conversely, studies in an oil channel are carried out in flow that is both highly viscous and slower moving. This allows for riblets to be made with spacings in the 3–10 mm range (Bechert *et al.* 1992).

Commercial and experimental application of riblets outside wind tunnels and test stands is also limited by the high costs for less-than-optimal riblet performance. Application of riblets on a large scale has been done for several

studies, as well as for competition and retail purposes. Sawtooth riblets on vinyl films produced by 3M riblets have been applied on surfaces ranging from boat hulls to airplanes. Racing swimsuits produced by Speedo and others also employ a riblet pattern on the surface to reduce drag during the streamline portion of each lap of a race (Krieger 2004). Additionally, a novel surface-scratching technique has been applied to the inside surface of pipelines to create a faux-riblet surface (Weiss 1997).

(*a*) *Riblet-dimension selection*

Though the turbulent-flow regime is characterized by completely random flow, the thickness of the viscous sublayer and the width of the streamwise vortices—and therefore the optimal riblet spacing—is dependent on properties of the fluid flow. Riblet spacing is the basis of other riblet dimensions, so the calculation of proper spacing is critical in riblet design. To calculate riblet spacing, wall shear stress must be known. Approximation of wall shear stress in rectangular channels can be done by combining the Blasius law for the friction coefficient with the Fanning friction factor and solving for wall shear stress. The Blasius law for the friction coefficient is defined as $c_f = 0.0791(Vd/\nu)^{-1/4}$, where ν is the kinematic viscosity and $d = 4A/p$ the hydraulic diameter of the channel, where A is the cross-sectional area and p the wetted perimeter. The Fanning friction factor is a dimensionless number defined as $c_f = 2\tau_0/\rho V^2$, where τ_0 is the wall shear stress, ρ the fluid density and V the average flow velocity. Combining equations, wall shear stress can be approximated by $\tau_0 = 0.03955\,\nu^{1/4}\rho\,V^{7/4}d^{-1/4}$.

Using the optimization comparison data in figure 7*a*, we know that a non-dimensionalized spacing should be chosen in the range $15 < s^+ < 18$. It is our recommendation that s^+ values for pipe flow be chosen slightly low, in the range $12 < s^+ < 14$, as shown in figure 12. To calculate physical spacing, s, from s^+, the non-dimensionalization factor, is used such that $s = s^+\nu/V_\tau$, where $V_\tau = (\tau_0/\rho)^{0.5}$ is the wall stress velocity. Using the optimization curves for each riblet shape in figure 6, the optimal spacing-based characteristic dimensions can be used to solve for optimal physical riblet dimensions.

(*b*) *Application of riblets for drag reduction*

The transition between research and application of technologies is often slow, and riblet surfaces have been no different. Because of the limitations of past riblet technologies, both benefit in commercial applications and the methods of application have been limited. Because riblets provide drag reduction on objects where the dominant form of drag is caused by turbulent flow at the surface, only objects of a certain form factor will show any measurable benefit. A large portion of the total drag on long objects with relatively flat sides usually comes from turbulence at the wall, so riblets will have an appreciable effect. However, for objects like automobiles, where pressure drag or flow separation is the dominant form of drag, application of riblets would have minimal effect.

Beginning in the mid-1980s, vinyl-film sawtooth riblets have been applied to boat hulls for racing. Both an Olympic rowing boat and an Americas Cup sailing yacht have been covered with riblets during competition. Riblets have also been

used on hulls of ships. Because skin friction of an aeroplane accounts for as much as 48 per cent of total drag, various studies to incorporate riblet structures on aircraft surfaces have been carried out at the National Aeronautics and Space Administration's Langley Research Center (USA) in the 1970s (Walsh & Anders 1989) and later at the German Aerospace Center (Bechert *et al.* 1997*a*). Vinyl-film riblets have also been applied to test planes of both Boeing and Airbus. These films have not seen use on standard commercial flights yet, but the benefits seen in testing should not go unmentioned. Application of riblets to an aeroplane requires that several concessions are made. Several locations that would be covered by riblets must be left uncovered owing to environmental factors; windows are not covered for the sake of visibility, several locations where dust and debris contacts the airplane during flight are left bare because the riblets would be eroded during flight, and locations where de-icing, fuel or hydraulic fluid would come in contact with the riblets are left bare. After these concessions, the riblets covering the remaining 70 per cent of the aircraft have provided 3 per cent total drag reduction. This 3 per cent drag reduction correlates to a similar 3 per cent savings in fuel costs (Bechert *et al.* 1997*a*). Another potential application of riblet structures in aeroplanes is on jet-engine blades to reduce skin friction.

Another large commercial application for riblet technologies is drag reduction in pipe flow. Machining the surface or applying vinyl-film riblets proves difficult in the confines of most pipes, and an alternate solution must be used. Experimental application of a scratching technique to the inside surface of pipes has created a riblet-like roughness that has provided more than 5 per cent drag-reduction benefit (Weiss 1997). Stemming from an old sailors' belief that ships sail faster when their hulls are sanded in the longitudinal direction, Weiss fabricated these riblets by using a steel brush moved through the pipeline to create a ridged surface. Studies have shown as much as a 10 per cent reduction in fluid flow with the combined effect of cleaning the pipe and ridging the surface. Tests on a 16 km gas-pipeline section have confirmed this benefit during commercial operation (Bechert *et al.* 1997*a*).

The dominant and perhaps only commercial market where riblet technology for drag reduction is commercially sold is competitive swimwear (Matthews 2008). The general population became aware of shark-skin's drag-reduction benefits with the introduction of the Fastskin suits by Speedo in 2004. Speedo claimed a drag reduction of several percent in a static test compared with other race suits. However, given the compromises of riblet geometry made during manufacturing, it is hard to believe the full extent of the drag reduction.

It is clear that creating surface structures by weaving threads is difficult. As a result, riblet geometries woven from thread have limited options of feasible riblet shapes. By the pattern woven into the Fastskin swimsuits, riblets are formed that resemble wide blade riblets with small grooves on top. The larger riblets are formed by the macro-weaving pattern, and the smaller riblets are created by the individual weaves of thread aligned with the macro-riblets. Both of these riblet-like shapes are distinguishable in figure 13. As shown in figure 13*a*, unstretched riblets are tightly packed. As the fabric stretches, the riblet width and spacing increase (figure 13*b*). The associated decrease in the h/s ratio depends on the dimensions of each swimmer's body, which is another compromising factor in the design. Riblet thickness is also a factor considered in the design.
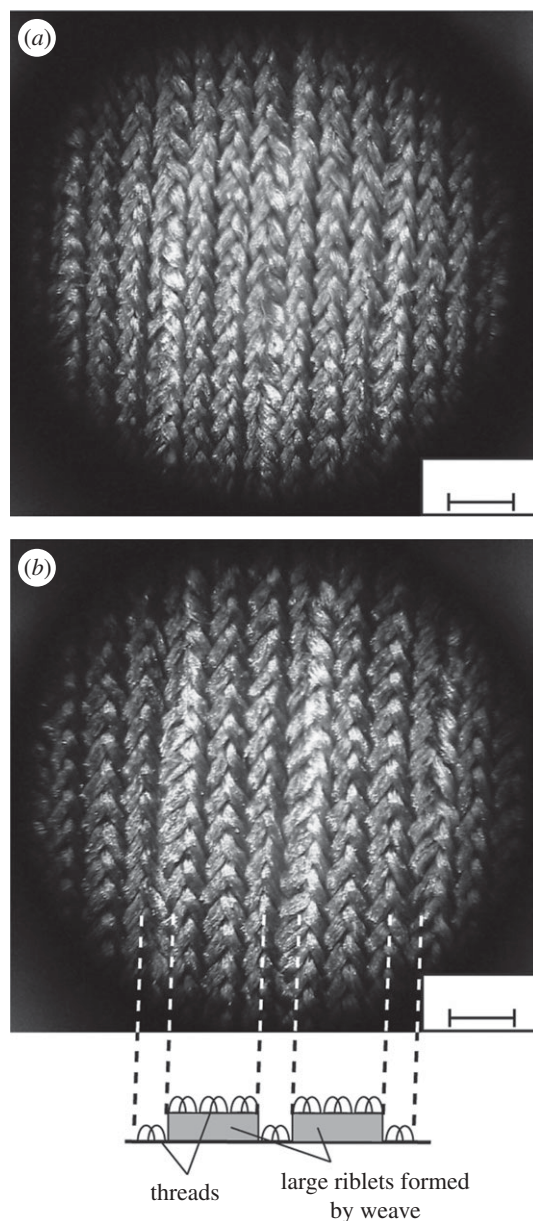
Figure 13. Images of riblet geometries on (*a*) unstretched (scale bar, 1.0 mm) and (*b*) stretched Speedo Fastskin swimsuit (scale bar, 1.0 mm) with a schematic showing apparent hierarchical riblet structure formed by threads.

Aside from the limitations imposed by the weaving patterns available, flexibility in the riblet tips will hinder the fabric's ability to impede the cross-stream translation of streamwise vortices. Thicker riblets are probably needed, used for strength, and cause a decrease in the peak drag-reduction capability compared with thinner riblets.

(c) *Riblet-fabrication methods for study and applications*

For experimentation, many riblet geometries have been made through careful machining of riblets from stock, but standard machining techniques lack the precision required to make riblets for use in high-speed air flow. Additionally, machining lacks the flexibility to fabricate small-scale riblets with enough resolution to create incrementally different samples for true optimization of sawtooth and scalloped riblets. Using a small-scale computer numerically controlled (CNC) mill, segmented-blade riblets have been fabricated in acrylic with a thickness of only 38 μm and a height of 90 μm (Jung & Bhushan 2010). Scalloped and sawtooth riblets have been machined in aluminium at spacings in the sub-millimetre range (Walsh & Lindemann 1984).

Another method used to construct blade riblets is to assemble separately fabricated parts. By fabricating thin element blades and spacers, stacked assemblies with adjustable geometry were created (Bechert *et al.* 1997*b*). By manufacturing blades in this separate manner, thinner blades can be fabricated using rolling techniques that eliminate the concern of milling errors ruining test plates. Riblet spacing is controlled by the added tolerances of each blade and spacer, which allows for an increase in overall fabrication tolerance. The major advantages of this method of assembly are ease of adjustment and less danger of milling errors destroying test plates. Optical images of assembled riblets can be seen in figure 9*a*.

For scale replicas and three-dimensional riblets, the complex shapes required usually afford moulding as the fabrication method. Micro-moulding and micro-embossing have been evaluated using polymethyl methacrylate (PMMA) as the mould material and a silicone rubber as the replica material (Xin & Zhang 2008). Replicas were shown to lack resolution by 2.2 and 5.5 per cent of the groove spacing and 8.3 and 5.9 per cent of the height, respectively. Alternatively, epoxy replicas of shark skin have been moulded in dental-wax reliefs taken from shark skin and studied in flow-cell experiments in a rectangular pipe section (Jung & Bhushan 2010). Scanning electron microscope (SEM) images of these replicas can be seen in figure 10*a*.

Many of these fabrication methods are not suitable for use outside laboratory settings. The wear experienced in a physical environment where riblets would provide measurable drag benefits would quickly render many of the above models non-beneficial. Additionally, fabrication for application on a large scale is a concern with most of these methods. Other methods of riblet manufacturing have been studied for use in production environments. 3M vinyl-film riblets have been used in myriad riblet-performance studies, and the fabrication of riblets by micro-profile grinding and incremental rolling processes have been investigated.

3M vinyl-film riblets (Marentic & Morris 1992) have been applied to many test surfaces, including the inner sides of various pipes for pipe-flow studies (Koury & Virk 1995), flat plates in flow channels and wind tunnels, boat hulls in towing tanks (Choi *et al.* 1989), aeroplane wings (Han *et al.* 2002) and aeroplane fuselages. Similar riblet films have been fabricated using bulk micro-machining of silicon to create a master for moulding of polydimethylsiloxane (PDMS) to create a thin, flexible riblet film. This film has been used in flow-visualization tests (Lee & Choi 2008).

Grinding and rolling methods of riblet fabrication have been studied for application in both research and large-scale application. A profiled grinding wheel has been used to fabricate several riblet geometries based on sawtooth riblets with $h = 20\,\mu m$ and $s = 50\,\mu m$ (Denkena *et al.* 2009). Dressing of the grinding wheel was done with a diamond-profile roller used in a two-step process in which the profile roller dresses every second tooth on the first pass, shifts axially the distance of one riblet spacing and dresses the remaining teeth on a second pass. One downside of the grinding process is the lack of hardening on the final riblet surface. Alternatively, rolling methods can be used to strain harden the riblets during fabrication. Using a roller with the profile of two riblets on its outer face, a linearly patterned rolling process has been used to fabricate scalloped riblets in a titanium alloy with $h = 162\,\mu m$ and $s = 340\,\mu m$ (Klocke *et al.* 2007). The strain hardening, favourable grain patterns and residual compressive stresses in the riblet surface after fabrication provide advantages in riblet strength for production applications.

6. Effect of slip length and polymer additives on fluid drag

Surfaces form molecular bonds with fluid molecules travelling across them. This attraction is not the same for all surface–fluid pairs, owing to the different chemical structures of different fluid molecules. For this reason, classical non-dimensionalization of these riblet tests does not allow for perfect comparison between studies done with different surface materials or fluids. Figure 14 shows a comparison between riblet performance studies that use similar riblet geometries tested with different surface-material–fluid pairs. It is clear that a similar behaviour is exhibited in both studies, but the curves do not match. The interactions between fluid molecules and the surface material, in addition to measurement resolution and accuracy, cause the experimental data to vary greatly at both the high and low ranges of s^+.

Another factor important to the drag experienced in fluid flow is the presence of polymer additives to the flow. The interaction between polymeric agents and the molecules of fluid in turbulent flow causes a large reduction in drag to occur. Fish secrete a small amount of mucus as they swim, which mixes with the fluid in the boundary layer and reduces the drag effects on the fish. Though sharks do not secrete enough mucus to use this mechanism for drag reduction, small amounts of mucus are present on the skin of sharks (Bechert *et al.* 1986).

(*a*) *The effect of fluid–surface bonding on drag reduction*

The degree to which bonding occurs between fluid molecules and the surface on which they rest can be described in many ways. The contact angle is the angle formed between the surface and the tangent line of a droplet where it contacts the surface. A perfect sphere of fluid on a surface has a contact angle of 180°, and a film of water has a contact angle of 0°. Another method of surface–fluid bonding characterization is the roll-off angle. This is the angle at which a drop of fluid previously at rest on a horizontal surface will move across a surface. Fluid molecules with a low affinity for inter-species bonding and a higher affinity for fluid–surface bonding will have a low contact angle and a high roll-off angle.
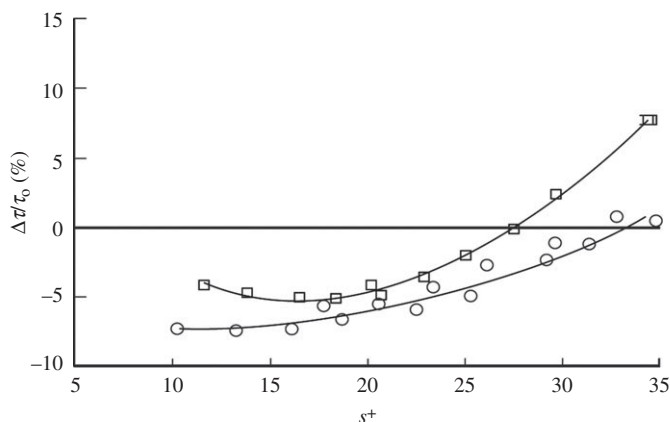
Figure 14. Comparison of drag reduction with oil (open squares) and air (open circles) on similar scalloped surfaces with $h/s = 0.5$ (adapted from Walsh (1982) and Bechert *et al.* (1997*b*)).

Fluids that have higher strength inter-species bonds than fluid–surface bonds will have high contact angles and low roll-off angles. The differences between the surface energy of the fluid molecules and the surface material alter the bonding tendencies. A surface that has lower surface energy than the fluid flowing over it will be less likely to bond with the fluid than a surface that has higher surface energy than the fluid above it. Two common fluids whose surface attraction properties are studied are water and oil. A surface that forms a contact angle with water less than 90° is said to be hydrophilic (water loving). If the same interface has a contact angle greater than 90°, it is said to be hydrophobic (water fearing). Surfaces with a contact angle greater than 150° are said to be superhydrophobic. To achieve superhydrophobicity, surface roughness must be applied in addition to typical material coatings. Surfaces that have the same contact-angle regimes when exposed to oil are said to be oleophilic, oleophobic or superoleophobic.

An obvious but often overlooked consequence of these fluid–surface interactions is fluid drag. A high roll-off angle is a sign that the apparent friction between the fluid and the surface is high. In a fluid flow, the classical no-slip condition at the surface is an effect of the attraction between molecules. However, it is possible to modify this boundary condition by changing the interaction between the surface and fluid. Water flowing over a hydrophobic surface will exhibit a velocity profile that seems to start from a non-zero number. Figure 15 shows a comparison of the velocity profile of a hydrophilic surface with a no-slip condition to the velocity profile of a hydrophobic surface with slip at the surface. The distance by which the apparent flow origin is below the surface is called the slip length. As the attraction between the fluid and surface is decreased, the slip length increases, and the fluid drag decreases.

The increase in initial velocity in pipe flow causes a corresponding increase in maximum flow velocity, and thus a decrease in drag. Pipes coated in low-surface-energy materials exhibit a decrease in pressure drop compared with similar pipes that have higher surface-energy coatings. Figure 16 shows laminar and turbulent pressure drop comparisons for a flow-cell experiment in which hydrophilic, hydrophobic and superhydrophobic surfaces in water flow. The greatest decrease
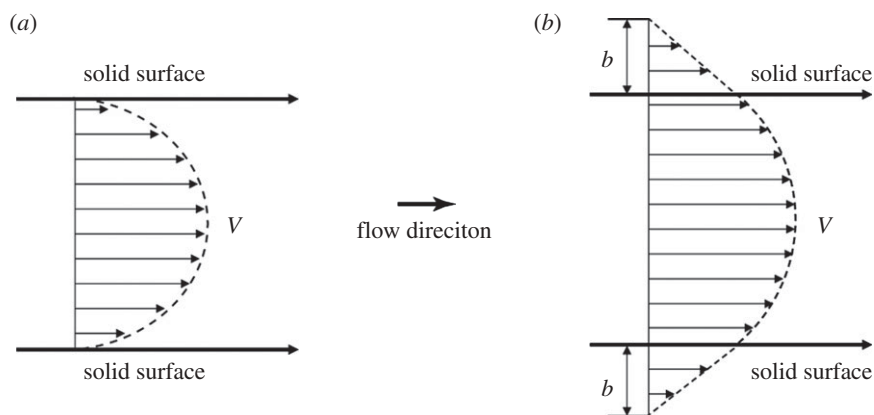
Figure 15. Schematic of velocity profiles without (a) and with (b) boundary slip. Slip length, b, occurs on hydrophobic surfaces (Jung & Bhushan 2010).
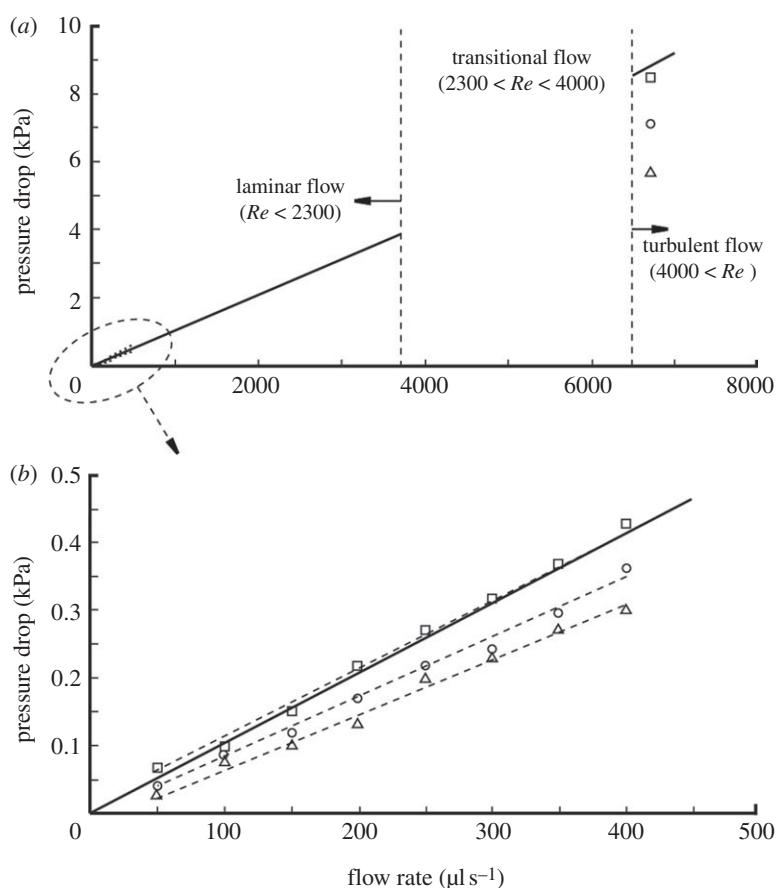

Figure 16. (a,b) Comparison of pressure drop in pipe flow of hydrophilic, hydrophobic and superhydrophobic surfaces in laminar- and turbulent-flow regimes. Decreased pressure drop in pipe flow corresponds to decreased drag (solid line, predicted for hydrophilic surface; open square, flat epoxy resin (hydrophilic); open circle, microstructure (hydrophobic); open triangle, hierarchical structure (superhydrophobic); adapted from Jung & Bhushan 2010).

in pressure drop and fluid drag happens for the superhydrophobic surface, on which a slip length of up to 100 µm was calculated (Ou *et al.* 2004; Jung & Bhushan 2010). This behaviour is similar for interactions between other fluid–surface pairs. Reducing the strength of bonding between the fluid molecules and the surface causes a corresponding reduction in fluid drag in both the laminar and turbulent regimes.

(b) Effect of fish mucus and polymers on fluid drag

Fish are known to secrete mucus during swimming. Though it is not known whether the mucus is present at all times, it is known that certain environmental factors cause, alter or enhance the production of mucus. These environmental stressors may present a need for increased swimming speed to catch or avoid becoming prey, protection against non-predatory threats such as micro-organisms, or resist abrasion while swimming near rocky surfaces. Regardless of which events cause fish to secrete mucus, the drag-reduction benefits during mucus-assisted swimming are known. Numerous experiments have demonstrated the drag reduction possible with fish-covered mucus compared with non-mucus-covered shapes (Hoyt 1975). In an experiment comparing the drag on wax models to a mucus-covered fish, a reduction in skin friction drag of 50 per cent was seen (Daniel 1981).

Similar to these fish-mucus experiments, polymer additives in pipe flows have been known for many years to reduce the drag in fluid flows by extreme amounts. In a pipe-flow study comparing various injection techniques of polymer solutions into water, drag reductions of up to 80 per cent were achieved (Frings 1988). Additionally, the drag-reduction benefit increases with increased Reynolds number. While this works well for pipe flows, in which the polymer remains mixed and active throughout the length of the pipe, its application to external flows is much more difficult. Mucus on fish does not mix well with water in static contact, but does mix and provide drag reduction during dynamic contact. By this feature, the mucus use of fish is minimized. Unfortunately, for any long-range application of polymer drag reduction on an external flow, the polymer solution must be continuously injected. This would cause large quantities of the solution to be used and probably render the strategy inefficient in terms of overall energy use.

Though sharks do not secrete enough mucus to use this mechanism for drag reduction, small amounts of mucus are present on the skin of sharks (Bechert *et al.* 1986). It is possible that shark-skin mucus secretion is similar to fish, where only environmental stressors or swimming cause an increase in output, but the total quantity of mucus on the surface at any given time is probably quite low. One possible mechanism by which this trace quantity of mucus could be useful is in changing the flow characteristics in the riblet valleys or at the riblet peaks, where shear stresses are highest. In the riblet valleys, a trace secretion of mucus could increase flow velocity and decrease the overall momentum transfer from the shark to the surrounding water by condensing the overall structure of the velocity gradient. Alternatively, injection at the riblet peaks may cause a reduction in shear stresses where they are at their maximum and again cause a reduction in drag. These small effects near the surface may propagate into a larger benefit as the lines of constant velocity in the flow shift and condense, as shown speculatively in figure 17. The localized effect of mucus secretion in the valleys or at the peaks
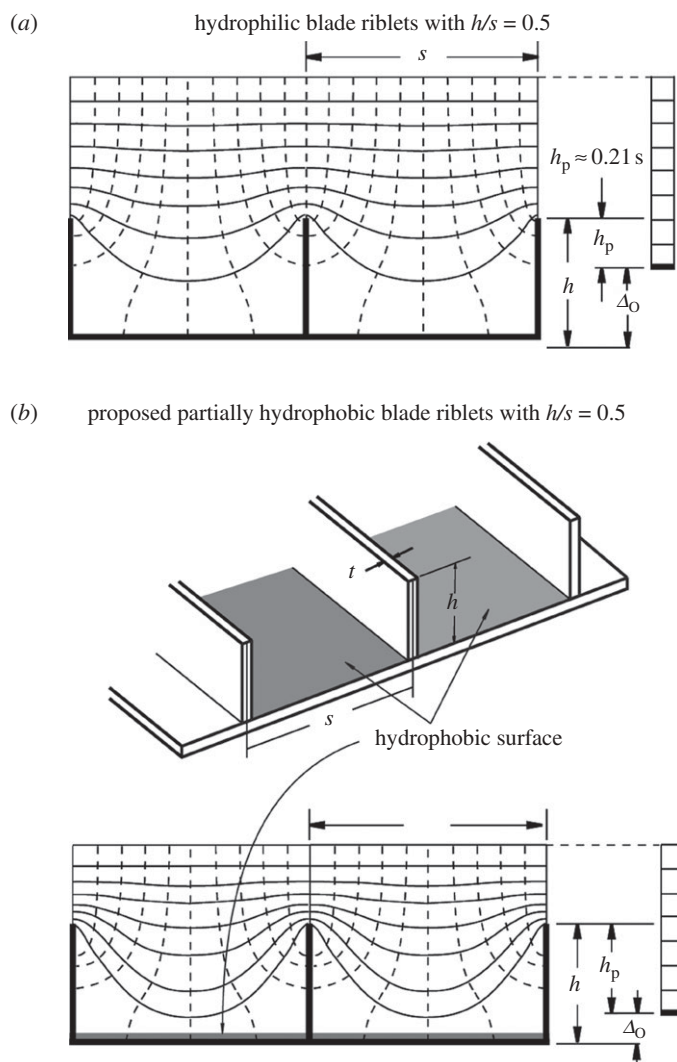
(*a*)   hydrophilic blade riblets with $h/s = 0.5$

(*b*)   proposed partially hydrophobic blade riblets with $h/s = 0.5$

Figure 17. (*a*) Behaviour of a hydrophilic surface in fluid flow ($h/s = 0.5$). (*b*) Proposed deposition of a hydrophobic surface on portions of a blade-riblet surface should increase the protrusion height of riblets and increase the drag-reduction benefit ($h/s = 0.5$).

would be similar to the effects of a partially hydrophobic surface. By coating a riblet surface with a hydrophobic layer in the valleys (figure 17*b*), at the peaks and as a whole, comparisons can be drawn between the drag-reduction effects of trace amounts of mucus found on shark skin.

7. Summary and outlook

Fluid drag in the turbulent boundary layer is, in a large part, owing to the effects of the streamwise vortices formed in the fluid closest to the surface. Turbulence and associated momentum transfer in the outer boundary layers is,

in a large part, owing to the translation, ejection and twisting of these vortices. Additionally, the vortices also cause high velocities at the surface that create large shear stresses on the surface. Numerical simulation has supported riblet drag-reduction theories by showing two mechanisms of riblet drag reduction. First, riblets impede the translation of the streamwise vortices, which causes a reduction in vortex ejection and outer-layer turbulence. Second, riblets lift the vortices off the surface and reduce the amount of surface area exposed to the high-velocity flow. By modifying the velocity distribution, riblets facilitate a net reduction in shear stress at the surface.

Various riblet shapes have been studied for their drag-reducing capabilities, but sawtooth, scalloped and blade riblets are most common. By varying flow properties or riblet geometries, optimization studies have been performed. Drag reduction by riblet surfaces has been shown to be as high as nearly 10 per cent given an optimal geometry of $h/s \sim 0.5$ for blade riblets with a no-slip condition. The maximum reliable drag reduction provided by scalloped riblets and sawtooth riblets is about 6 per cent at $h/s \sim 0.7$ and 5 per cent at $\alpha \sim 60°$, respectively. Experimentation of other shapes has provided similar benefits of around 5 per cent drag reduction. Additional experimentation with simple three-dimensional shapes, such as offset segmented-blade riblets, has shown a comparable performance to standard-blade riblets, but hierarchical structures and complex three-dimensional shapes have yet to show improved benefits. The behaviour of static and dynamic versions of complex three-dimensional replicas has been minimally investigated, and much work remains in understanding the complexities that are involved. To date, no improved drag reduction has been accomplished using replica models, but hypothesized control mechanisms for dynamic replicas have been proposed. Though the optimum shape for drag-reduction performance is blade riblets, the fragile nature of these blades makes their commercial application of little use. Scalloped and sawtooth riblets, which provide considerably less drag-reduction benefits, are much stronger shapes mechanically speaking and should be used for application in environments where contact may occur with non-fluid materials.

Commercial applications of riblets include competition swimsuits, which use a thread-based riblet geometry, as well as experimental applications to aeroplanes. Drag reductions in riblet application have been accomplished, and flight applications have seen a fuel saving of as much as 3 per cent. Manufacturing techniques for riblets must also be chosen specific to their application. Vinyl-film riblets are the easiest method, as application of a film to a surface requires less for work small-scale application than other methods. Rolling or grinding methods of riblet application should be investigated for turbine blades or high-volume commercially sold pieces. Machining methods are unfavourable in most instances, and should be avoided in most instances of non-research riblet application.

The future of riblet research is two-fold. The investigation of both static and dynamic riblet-topped scales, as well as partially-to-fully fluid-bond-resistant riblet surfaces must be investigated. Application of superhydrophobic surfaces to riblet geometries should be investigated in a flow-cell experiment using water to study the effects of localized hydrophobicity on water flow over riblets. We expect that a notable increase in drag reduction will be seen using a biomimetic application of hydrophobic surfaces at the riblet valleys, the riblet peaks, or alternatively across the entire surface. Additionally, atomic

force microscope studies of the nanoscale surface characteristics on shark skin should be done to investigate the possibility of nano-roughness improving the overall hydrophobicity of the shark-skin surface. We expect that in combination and separate, the mucus and surface-roughness characteristics of the shark skin will provide increased drag-reduction benefits compared with current fabricated surfaces.

References

Bechert, D. W. & Hoppe, G., 1985 On the drag reduction of the shark skin. In *AIAA Shear Flow Control Conf., Boulder, CO, 12–14 March*, paper no. AIAA-85-0564.

Bechert, D. W., Bartenwerfer, M., Hoppe, G. & Reif, W.-E. 1986 Drag reduction mechanisms derived from shark skin. In *Proc. 15th Int. Council of Aeronautical Sciences Congress, London, UK, 7–12 September*, vol. 2, pp. 1044–1068, paper no. ICAS-86-1.8.3.

Bechert, D. W., Hoppe, G., van der Hoven, J. G. Th. & Makris, R. 1992 The Berlin oil channel for drag reduction research. *Exp. Fluids* **12**, 251–260. (doi:10.1007/BF00187303)

Bechert, D. W., Bruse, M., Hage, W. & Meyer, R. 1997a Biological surfaces and their technological application—laboratory and flight experiments on drag reduction and separation control. In *AIAA 28th Fluid Dynamics Conference, Snowmass Village, CO, 29 June–2 August*, paper no. AIAA-1997-1960.

Bechert, D. W., Bruse, M., Hage, W., van der Hoeven, J. G. T. & Hoppe, G. 1997b Experiments on drag reducing surfaces and their optimization with an adjustable geometry. *J. Fluid Mech.* **338**, 59–87. (doi:10.1017/S0022112096004673)

Bechert, D. W., Bruse, M. & Hage, W. 2000a Experiments with three-dimensional riblets as an idealized model of shark skin. *Exp. Fluids* **28**, 403–412. (doi:10.1007/s003480050400)

Bechert, D. W., Bruse, M., Hage, W. & Meyer, R. 2000b Fluid mechanics of biological surfaces and their technological application. *Naturwissenschaften* **87**, 157–171. (doi:10.1007/s001140050696)

Bhushan, B. 2007 Adhesion of multi-level hierarchical attachment systems in gecko feet. *J. Adhesion Sci. Technol.* **21**, 1213–1258. (doi:10.1163/156856107782328353)

Bhushan, B. 2008 *Nanotribology and nanomechanics—an introduction*, 2nd edn. Heidelberg, Germany: Springer.

Bhushan, B. 2009 Biomimetics: lessons from nature—an overview. *Phil. Trans. R. Soc. A* **367**, 1445–1486. (doi:10.1098/rsta.2009.0011)

Bhushan, B. 2010 *Springer handbook of nanotechnology*, 3rd edn. Heidelberg, Germany: Springer. (doi:10.1007/978-3-642-02525-9)

Bhushan, B. & Her, E. K. 2010 Fabrication of superhydrophobic surfaces with high and low adhesion inspired from rose petal. *Langmuir* **26**, 8207–8217. (doi:10.1021/la904585j)

Choi, K. S., Gadd, G. E., Pearcey, H. H., Savill, A. M. & Svensson, S. 1989 Tests of drag-reducing polymer coated on a riblet surface. *Appl. Sci. Res.* **46**, 209–216. (doi:10.1007/BF00404818)

Choi, K. S., Yang, X., Clayton, B. R., Glover, E. J., Altar, M., Semenov, B. N. & Kulik, V. M. 1997 Turbulent drag reduction using compliant surfaces. *Proc. R. Soc. A* **453**, 2229–2240. (doi:10.1098/rspa.1997.0119)

Coles, D. 1978 A model for flow in the viscous sublayer. In *Proc. Workshop on Coherent Structure of Turbulent Boundary Layers, Bethlehem, PA,* pp. 462–475.

Cutkosky, M. R. & Kim, S. 2009 Design and fabrication of multi-material structures for bioinspired robots. *Phil. Trans. R. Soc. A* **367**, 1799–1813. (doi:10.1098/rsta.2009.0013)

Daniel, T. L. 1981 Fish mucus: *in situ* measurements of polymer drag reduction. *Biol. Bull.* **160**, 376–382. (doi:10.2307/1540846)

Denkena, B., de Leon, L. & Wang, B. 2009 Grinding of microstructured functional surfaces: a novel strategy for dressing of microprofiles. *Prod. Eng.* **3**, 41–48. (doi:10.1007/s11740-008-0134-0)

Frings, B. 1988 Heterogeneous drag reduction in turbulent pipe flows using various injection techniques. *Rheologica Acta* **27**, 92–10. (doi:10.1007/BF01372455)

Goldstein, D., Handler, R. & Sirovich, L. 1995 Direct numerical simulation of turbulent flow over a modeled riblet covered surface. *J. Fluid Mech.* **302**, 333–376. (doi:10.1017/S0022112095004125)

Gorb, S. 2001 *Attachment devices of insect cuticles.* Dordrecht, The Netherlands: Kluwer.

Han, M., Huh, J. K., Lee, S. S. & Lee, S. 2002 Micro-riblet film for drag reduction. In *Proc. Pacific Rim Workshop on Transducers and Micro/Nano Technologies, Xiamen, China.*

Hoyt, J. W. 1975 Hydrodynamic drag reduction due to fish slimes. *Swimming and Flying in Nature* **2**, 653–672.

Jung, Y. C. & Bhushan, B. 2010 Biomimetic structures for fluid drag reduction in laminar and turbulent flows. *J. Phys.: Condens. Matter* **22**, 035104. (doi:10.1088/0953-8984/22/3/035104)

Kline, S. J., Reynolds, W. C., Schraub, F. A. & Runstadler, P. W. 1967 The structure of turbulent boundary layers. *J. Fluid Mech.* **30**, 741–773. (doi:10.1017/S0022112067001740)

Klocke, F., Feldhaus, B. & Mader, S. 2007 Development of an incremental rolling process for the production of defined riblet surface structures. *Prod. Eng.* **1**, 233–237. (doi:10.1007/s11740-007-0031-y)

Koury, E. & Virk, P. S. 1995 Drag reduction by polymer solutions in a riblet-lined pipe. *Appl. Sci. Res.* **54**, 323–347. (doi:10.1007/BF00863517)

Krieger, K. 2004 Do pool sharks really swim faster? *Science* **305**, 636–637. (doi:10.1126/science.305.5684.636)

Lang, A. W., Motta, P., Hidalgo, P. & Westcott, M. 2008 Bristled shark skin: a microgeometry for boundary layer control? *Bioinspir. Biomim.* **3**, 1–9. (doi:10.1088/1748-3182/3/4/046005)

Lee, S. J. & Choi, Y. S. 2008 Decrement of spanwise vortices by a drag-reducing riblet surface. *J. Turbul.* **9**, 1–15. (doi:10.1080/14685240802251517)

Lee, S.-J. & Lee, S.-H. 2001 Flow field analysis of a turbulent boundary layer over a riblet surface. *Exp. Fluids* **30**, 153–166. (doi:10.1007/s003480000150)

Liu, K. N., Christodoulou, C., Riccius, O. & Joseph, D. D. 1990 Drag reduction in pipes lined with riblets. *AIAA J.* **28**, 1697–1699. (doi:10.2514/3.10459)

Matthews, J. N. A. 2008 Low-drag suit propels swimmers. *Physics Today*, August, pp. 32–33.

Marentic, F. J. & Morris, T. L. 1992 *Drag reduction article.* United States Patent no. 5 133 516.

Munson, B., Young, D. & Okiishi, T. 2005 *Fundamentals of fluid mechanics*, 5th edn. New York, NY: Wiley.

Nosonovsky, M. & Bhushan, B. 2008 *Multiscale dissipative mechanisms and hierarchical surfaces: friction, superhydrophobicity, and biomimetics.* Heidelberg, Germany: Springer.

Ou, J., Perot, B. & Rothstein, J. P. 2004 Laminar drag reduction in microchannels using ultrahydrophobic surfaces. *Phys. Fluids* **16**, 4635–4643. (doi:10.1063/1.1812011)

Reif, W.-E. 1985 *Squamation and ecology of sharks*, vol. 78, pp. 1–255. Frankfurt, Germany: Courier Forschungsinstitut Senckenberg.

Robinson, S. K. 1991 *The kinematics of turbulent boundary layer structure.* NASA TM 103859, NASA, Washington, DC.

Rohr, J. J., Anderson, G. W., Reidy, L. W. & Hendricks, E. W. 1992 A comparison of the drag-reducing benefits of riblets in internal and external flows. *Exp. Fluids* **13**, 361–368. (doi:10.1007/BF00223243)

Shephard, K. L. 1994 Functions for fish mucus. *Rev. Fish Biol. Fish.* **4**, 401–429. (doi:10.1007/BF00042888)

Walsh, M. J. 1980 Drag characteristics of v-groove and transverse curvature riblets. *Viscous Flow Drag Reduction* **72**, 169–184.

Walsh, M. J. 1982 Turbulent boundary layer drag reduction using riblets. In *AIAA 20th Aerospace Sciences Meeting, Orlando, FL, 11–14 January*, paper no. AIAA-82-0169.

Walsh, M. J. & Anders, J. B. 1989 Riblet/LEBU research at NASA Langley. *Appl. Sci. Res.* **46**, 255–262. (doi:10.1007/BF00404822)

Walsh, M. J. & Lindemann, A. M. 1984 Optimization and application of riblets for turbulent drag reduction. In *AIAA 22nd Aerospace Sciences Meeting, Reno, NV, 9–12 January*, paper no. AIAA-84-0347.

Weiss, M. H. 1997 Implementation of drag reduction techniques in natural gas pipelines. In *10th European Drag Reduction Working Meeting, Berlin, Germany, 19–21 March.*

Wilkinson, S. P. 1983 Influence of wall permeability on turbulent boundary-layer properties. In *21st Aerospace Sciences Meeting of the American Institute of Aeronautics and Astronautics, Reno, NV, 10–13 January*, paper no. AIAA 83-0294.

Wilkinson, S. P. & Lazos, B. S. 1987 Direct drag and hot-wire measurements on thin-element riblet arrays. In *IUTAM Symposium on Turbulence Management and Relaminarization, Bangalore, India, 19–23 January.*

Wilkinson, S. P., Anders, J. B., Lazos, B. S. & Bushnell, D. M. 1988 Turbulent drag reduction research at NASA Langley: progress and plans. *Inter. J. Heat Fluid Flow* **9**, 266–277. (doi:10.1016/0142-727X(88)90037-9)

Xin, H. & Zhang, D. 2008 Study on the micro-replication of shark skin. *Sci. China Ser. E: Technol. Sci.* **51**, 890–896. (doi:10.1007/s11431-008-0080-2)

CORRECTION

Shark-skin surfaces for fluid-drag reduction in turbulent flow: a review

By Brian Dean and Bharat Bhushan

Figure 7a was presented incorrectly in our paper (Dean & Bhushan 2010). The corrected figure is presented below. The caption for figure 7 remains the same.